PHYSICAL REVIEW E **76**, 015301(R) (2007)

Controlling the stability transfer between oppositely traveling waves and standing waves by inversion-symmetry-breaking perturbations

A. Pinter,* M. Lücke, and Ch. Hoffmann
Institut für Theoretische Physik, Universität des Saarlandes, Postfach 151150, D-66041 Saarbrücken, Germany
(Received 14 November 2006; published 6 July 2007)

The effect of an externally applied flow on symmetry degenerated waves propagating into opposite directions and standing waves that exchange stability with the traveling waves via mixed states is analyzed. Wave structures that consist of spiral vortices in the counter rotating Taylor-Couette system are investigated by full numerical simulations and explained quantitatively by amplitude equations containing quintic coupling terms. The latter are appropriate to describe the influence of inversion-symmetry-breaking perturbations on many oscillatory instabilities with O(2) symmetry.

DOI: 10.1103/PhysRevE.76.015301 PACS number(s): 47.20.Ky, 47.32.−y, 47.54.−r

Many nonlinear structure forming systems that are driven out of equilibrium show a transition to traveling waves (TWs) as a result of an oscillatory instability [1]. Also, in the presence of inversion symmetry in one or two spatial directions a standing wave (SW) solution bifurcates in addition to the symmetry degenerate, oppositely propagating TWs at the same threshold. Moreover, depending on the parameters one can have a stability exchange between TWs and SWs as the driving rate varies. The stability transfer is mediated by mixed patterns that establish in the solution space a connection between a pure TW and a pure SW.

Here we investigate how externally tunable symmetry-breaking perturbations change stability, bifurcation properties, and the spatiotemporal behavior of the aforementioned structures. To be concrete, we investigate vortex waves in the annular gap between counter-rotating concentric cylinders of the Taylor-Couette system [2,3]. To that end we performed full numerical simulations of the Navier-Stokes equations with the methods described in [4]. We elucidate that and how these results can be explained quantitatively by amplitude equations which contain only quintic order terms.

The perturbation is realized in our system by an externally enforced axial through flow that can easily be controlled experimentally. However, our results concerning the influence of inversion-symmetry-breaking perturbations on TWs, SWs, and on the mixed states are more general: the quintic order amplitude equations with small symmetry-breaking terms apply to all kinds of O(2) symmetric oscillatory instabilities in the presence of inversion-symmetry-breaking perturbations.

Structures. Without symmetry breaking through flow the following oscillatory vortex structures occur at small driving [5,6]: (i) Forward bifurcating TWs consisting of left-handed spiral vortices (L-SPI) or of right-handed spiral vortices (R-SPI) that are mirror images of each other. L-SPI (R-SPI) travel in the annulus between the two cylinders into (opposite to) the direction of the rotation frequency vector of the inner one, i.e., in our notation upwards (downwards) [4]. (ii) Forward bifurcating SWs that consist of an equal-amplitude nonlinear combination of L-SPI and R-SPI that are called ribbons (RIBs) in the Taylor-Couette literature [7,8]. (iii) So-called cross spirals (CR-SPI), i.e., combinations of L-SPI and R-SPI with different amplitudes. They provide a stability transferring connection between TW and SW solution branches [3,6]. The vortex structures (i)–(iii) are axially and azimuthally periodic with wave numbers $k=2\pi/\lambda$ and M, respectively, with $\lambda=1.3$ and $M=2$ throughout this paper. They rotate with characteristic constant angular velocities as a whole into the same direction as the inner cylinder [4]. Thereby they are forced to propagate axially with the exception of RIB vortices which rotate only and do not propagate.

Order parameters. Figures 1 and 2 show bifurcation diagrams of SPI, CR-SPI, and RIB solutions in a system of radius ratio $\eta=1/2$ for fixed $R_1=240$ versus the reduced distance $\mu=(R_2-R_2^0)/|R_2^0|$ from the spiral onset R_2^0. Here, R_1 and R_2 are the Reynolds numbers defined by the rotational velocities of the inner and outer cylinder, respectively, and Re is the Reynolds number of the imposed axial through flow. In Figs. 1 and 2, the influence of a small through flow (Re $=0.02$) is compared with the situation without through flow. Order parameters in Fig. 1 are the squared amplitudes $|A|^2, |B|^2$ of the dominant critical modes

$$u_{2,1}(t) = |A|e^{-i\omega_A t}, \quad u_{2,-1}(t) = |B|e^{-i\omega_B t} \tag{1}$$

in the double Fourier decomposition of the radial velocity u at midgap in azimuthal and axial direction. The indices 2 and ± 1 identify azimuthal and axial modes, respectively. The linear stability analysis of the basic state consisting of a superposition of circular Couette flow and of annular Poiseuille flow in axial direction shows that the growth rates of these modes become positive at the respective bifurcation thresholds μ_A and μ_B of $M=2$ L-SPI and R-SPI, respectively. Note also that for all relaxed vortex structures investigated here the moduli and frequencies of $u_{2,\pm 1}$ in Eq. (1) are constant.

In Fig. 2 we show, in addition, the bifurcation diagrams of the combinations

$$S = (|A|^2 + |B|^2)/2, \quad D = (|A|^2 - |B|^2)/2 \tag{2}$$

since they are convenient to describe in particular CR-SPI.

Bifurcation scenario for zero through flow. In the symmetry degenerate case without through flow L-SPI ($A \neq 0 = B$, $D>0$) and R-SPI ($A=0\neq B$, $D<0$) have identical bifurca-

*kontakt@alexander-pinter.de

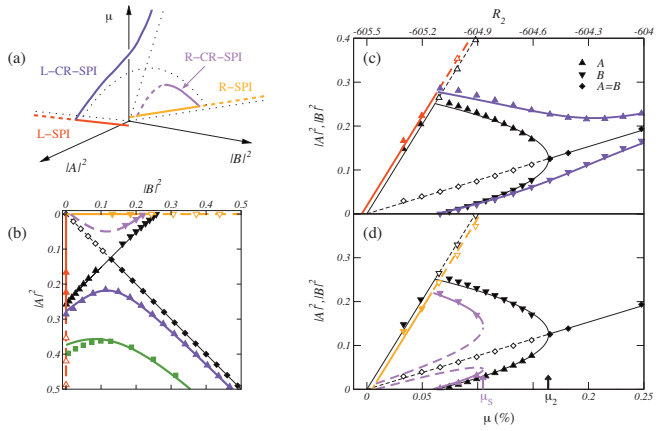

FIG. 1. (Color) Bifurcation diagrams of L-SPI ($A \neq 0$, $B=0$, $D>0$), R-SPI ($A=0$, $B \neq 0$, $D<0$), L-CR-SPI ($|A|>|B|$, $D>0$), R-CR-SPI ($|B|>|A|$, $D<0$), and RIB ($A=B$, $D=0$—only for Re $=0$) as functions of μ and R_2 for $R_1=240$. Here, A and B are the amplitudes of the dominant modes $u_{2,1}(t)$ and $u_{2,-1}(t)$ Eq. (1), respectively, in the radial velocity field u at midgap. Solid (open) symbols denote stable (unstable) solutions of the full Navier-Stokes equations. Full (dashed) lines are the stable (unstable) solutions of the coupled amplitude equations. Red, orange, violet, and magenta show results for Re=0.02. The color coding of the different solutions is given in the schematic three-dimensional bifurcation diagram of (a). Therein the black dots denote Re=0 solutions without stability information. In (b) we show the projection of bifurcation diagrams onto the $|A|^2-|B|^2$ plane. The color green refers to L-CR-SPI for Re=0.1 where R-CR-SPI do not exist anymore. Black symbols and lines in (b)–(d) refer to Re=0.

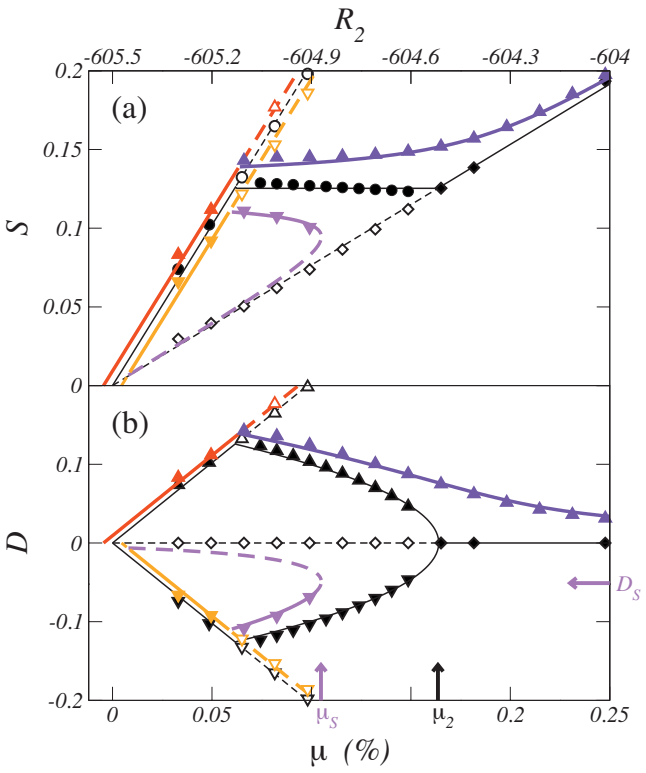

FIG. 2. (Color) Bifurcation behavior of the vortex states of Fig. 1 are shown here in plots of (a) S and (b) D versus μ and R_2, respectively. The color coding is the same as in Fig. 1.

tion properties. They are stable close to onset, whereas RIB ($A=B$, $D=0$) are initially unstable. In the driving range shown in Figs. 1 and 2 the squared amplitudes of these two states grow practically linearly with the reduced distance μ from the common onset at $\mu=0$, albeit with different slopes. Then, there appear in a finite supercritical driving interval stable CR-SPI solutions which transfer stability from SPI to RIB. The solution which bifurcates with $B=0$ out of the L-SPI is identified as a L-CR-SPI with $|A|>|B|$, i.e., $D>0$. The symmetry degenerate R-CR-SPI ($|B|>|A|$, $D<0$) bifurcates with $A=0$ out of the R-SPI. In the former $|B|$ grows and $|A|$ decreases—and vice versa in the latter—until the CR-SPI branches end with $A=B$, $D=0$ in the RIB solution. The amplitude variations of the CR-SPI solutions, however, are such that the sum S remains practically constant, cf. Fig. 2(a). The RIB state loses stability outside the plot range of Figs. 1 and 2 to another type of amplitude-modulated CR-SPI that are not discussed here.

Through-flow-induced changes. The axial through flow significantly perturbs and changes structure, dynamics, and bifurcation behavior of the SPI vortex solutions discussed so far [4,9–12]: RIBs cease to exist in the strict sense, L-SPI and R-SPI are no longer mirror images of each other, and also L-CR-SPI are no longer related to R-CR-SPI by this symmetry operation. However, spirals retain their spatiotemporal structure in the through flow, i.e., they still do not depend on φ, z, t separately, but only on the phase combination $\phi_A=M\varphi+kz-\omega_A t$ or $\phi_B=M\varphi-kz-\omega_B t$, respectively. L-SPI (red in Figs. 1 and 2) bifurcate for small Re>0 at a threshold value $\mu_A<0$ prior to R-SPI (orange), which bifurcate at $0<\mu_B \approx -\mu_A$ out of the basic state.

L-SPI are again stable at onset, but then lose stability to L-CR-SPI (violet) which remain stable in the plotted parameter regime. The L-CR-SPI solution approaches the (Re=0) RIB state with increasing μ, but retains with $A \neq B$ a finite distance $D>0$. On the other hand, R-SPI are unstable for small and large μ, but stable for intermediate μ. Stability is exchanged with a R-CR-SPI (magenta) which has a stable as well as an unstable branch resulting from a saddle-node bifurcation at μ_S in Figs. 1 and 2. For small μ the unstable R-CR-SPI lies close to the (Re=0) RIB solution and bifurcates with finite $D<0$ out of the R-SPI slightly above μ_B. Note also that the sum of the squared amplitudes S of CR-SPI is no longer constant as for the case of Re=0.

Amplitude equations. The changes in spatiotemporal, bifurcation, and stability behavior of SPI, CR-SPI, and RIB states by a small through flow can be explained and described close to onset quantitatively within an amplitude-equation approach. To demonstrate that we focus here on the bifurcation properties of the moduli $|A|, |B|$ of the critical modes.

In order to reproduce the bifurcation and stability behavior of the aforementioned vortex states, including the CR-SPI, one needs coupled equations for A and B of at least quintic order. Higher-order terms that are suggested in [3] are not necessary to ensure the existence of CR-SPI solutions. Symmetry arguments [3,6,9] restrict the form of the equations for the moduli to

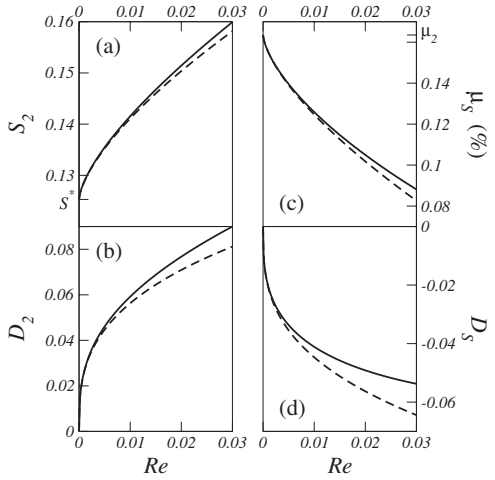

FIG. 3. Power-law behavior of quantities characterizing the breakup of the Re=0 pitchfork bifurcation from RIB to CR-SPI versus through-flow strength Re for $R_1=240$. D_2 and S_2 refer to values at the location μ_2 of the unperturbed bifurcation; D_S and μ_S are saddle node coordinates, cf. Fig. 2(b). Solid lines come from the full fixed point equations (5); dashed lines refer to their leading order approximations, Eqs. (6) and (7).

$$\tau_A \frac{d|A|}{dt} = |A|[(\mu - \mu_A) + b_A|A|^2 + c_A|B|^2 + e_A(|A|^2|B|^2 - |B|^4)], \tag{3a}$$

$$\tau_B \frac{d|B|}{dt} = |B|[(\mu - \mu_B) + b_B|B|^2 + c_B|A|^2 + e_B(|B|^2|A|^2 - |A|^4)], \tag{3b}$$

with real coefficients that depend in general on Re. Here we have discarded the quintic terms $|A|^5$ and $|B|^5$ in view of the linear variation of the squared SPI moduli with μ, cf. Fig. 1. Furthermore, we made a special choice for the coefficients of the last terms $|A||B|^4$ and $|B||A|^4$ in Eq. (3) that is motivated by the linear variation of the squared RIB moduli with μ for Re=0 and that suffices to describe the behavior for small Re as well.

Coefficients. As a result of the inversion symmetry under $z \leftrightarrow -z$, which includes reverting the through flow, the coupled equations are invariant under the operation $(A,B,\mathrm{Re}) \leftrightarrow (B,A,-\mathrm{Re})$ so that the coefficients in Eq. (3) obey relations such as, e.g., $c_A(\mathrm{Re})=c_B(-\mathrm{Re})$. To reproduce the bifurcation properties of the moduli for small Re as in Figs. 1 and 2 it suffices to incorporate the Re dependence to linear order in the coefficients

$$\mu_A(\mathrm{Re}) = -\mu^{(1)}\,\mathrm{Re}, \quad \mu_B(\mathrm{Re}) = \mu^{(1)}\,\mathrm{Re} \tag{4a}$$

$$c_A(\mathrm{Re}) = c + c^{(1)}\,\mathrm{Re}, \quad c_B(\mathrm{Re}) = c - c^{(1)}\,\mathrm{Re} \tag{4b}$$

only and to ignore any Re dependence of the others by setting

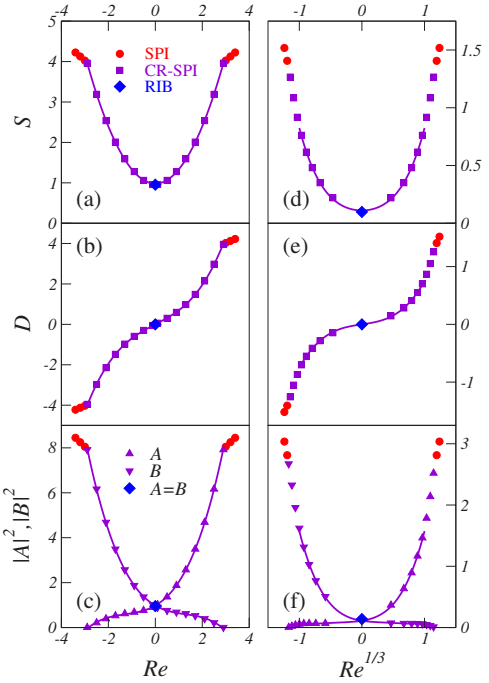

FIG. 4. (Color online) Power-law variation of S, D, $|A|^2=S+D$, $|B|^2=S-D$ with through-flow Re during the transformation from RIB (diamond) at Re=0 to CR-SPI (squares and triangles). The latter undergo a transition to SPI (circles) at large Re. Symbols denote results from the full Navier-Stokes equations for $R_1=240$, lines show fits explained in the text. Right column: $\mu=\mu_2$, i.e., the unperturbed pitch fork location; left column $\mu=0.011$, i.e., far away from it. Note the different abscissa scaling of the two columns.

$$b_A = b_B = b, \quad e_A = e_B = e. \tag{4c}$$

The choice $b_A=b_B=b$ reflects the fact that the linear growth of the squared SPI moduli with the distance from their respective thresholds at μ_A and μ_B is unchanged by the through flow. On the other hand, the downwards shift of the L-SPI onset being for small through flow of equal magnitude as the upwards shift of the R-SPI onset is reflected by $\mu_A(\mathrm{Re})=-\mu_B(\mathrm{Re})=-\mu^{(1)}\,\mathrm{Re}$ with positive $\mu^{(1)}$. The coupling constant $e_A=e_B=e$ ensures the existence of CR-SPI solutions [6]. The flow-induced changes of the coupling constants c_A and c_B reflect the perturbation and destruction of the RIB states and ensures for positive Re L-CR-SPI solutions with $D>0$ when μ is large. The values of the coefficients [13] were obtained from linear stability analyses and by fits to the full numerical nonlinear results.

Fixed points. With the coefficients (4) it is straightforward to derive from Eq. (3) the following relations for the fixed points of S and D:

$$\mu + (b+c)S - c^{(1)}\,\mathrm{Re}\,D - 2eD^2 = 0, \tag{5a}$$

$$\mu^{(1)}\,\mathrm{Re} + (b-c)D + c^{(1)}\,\mathrm{Re}\,S + 2eSD = 0. \tag{5b}$$

From these equations we have obtained the lines in the bifurcation plots of $|A|^2=S+D$ and $|B|^2=S-D$ in Fig. 1 and of S and D in Fig. 2. They compare very well with the symbols from the full numerical simulations of the Navier-Stokes

equations, say, up to $\mathrm{Re} \simeq 0.2$ or so. Beyond that higher order terms in the Re expansion of the coefficients should be included.

Perturbation of the RIB $\rightarrow$ CR-SPI *bifurcation*. The black lines and symbols in Figs. 1 and 2 show that without through flow the RIB state which is stable at large μ transfers stability to CR-SPI in a pitchfork bifurcation located at μ_2 in Figs. 1 and 2. The symmetry and topology of this unperturbed bifurcation out of the $D=0$ RIB solution at $\mu_2=-(b+c)S_*$, $S_*=(c-b)/(2e)$ is best seen in Fig. 2(b). This figure shows also most clearly how the through flow with $\mathrm{Re}>0$ perturbs this bifurcation into a continuously varying stable solution branch with $D>0$ (violet) and a pair of stable and unstable solutions (magenta) that are connected by a saddle-node bifurcation at μ_S.

The values of S and D at the unperturbed location $\mu=\mu_2$ of the pitchfork bifurcation

$$S(\mu_2) = S_2 = S_* + \hat{s}_2\,\mathrm{Re}^{2/3} + \text{h.o.t.}, \tag{6a}$$

$$D(\mu_2) = D_2 = \hat{d}_2\,\mathrm{Re}^{1/3} + \text{h.o.t.} \tag{6b}$$

grow $\propto \mathrm{Re}^{2/3}$ and $\propto \mathrm{Re}^{1/3}$, respectively, with constants $\hat{d}_2^3=-(b+c)(\mu^{(1)}+c^{(1)}S_*)/(4e^2)$ and $\hat{s}_2=2e\hat{d}_2^2/(b+c)$. The coordinates of the saddle-node bifurcation, as indicated in Fig. 2(b) by the magenta arrows,

$$\mu_S = \mu_2 + \hat{\mu}_S\,\mathrm{Re}^{2/3} + \text{h.o.t.}, \quad D_S = \hat{d}_S\,\mathrm{Re}^{1/3} + \text{h.o.t.}, \tag{7}$$

vary $\propto \mathrm{Re}^{2/3}$ and $\propto \mathrm{Re}^{1/3}$ with the perturbation strength Re. Here the constants are $\hat{d}_S^3=[(c^2-b^2)c^{(1)}+2e(b+c)\mu^{(1)}]/(16e^3)$ and $\hat{\mu}_S=[(b+c)\mu^{(1)}-\mu_2 c^{(1)}+4e^2\hat{d}_S^3]/(2e\hat{d}_S)$. The comparison in Fig. 3 of these lowest order approximations [Eqs. (6) and (7)] that reflect an additive pitchfork unfolding with the full fixed point result from Eq. (5) shows good agreement for $\mathrm{Re} \lesssim 0.02$.

Larger through flow. Here we investigate the transformation of the unperturbed RIB state into a CR-SPI as a function of the through-flow strength extending to larger Reynolds numbers up to $\mathrm{Re}=4$, which are about 200 times larger than those studied so far in this paper. For such large Re the amplitude equations with the simple Re dependence of the coefficients (4) are no longer adequate to describe the behavior of the order parameters S and D. However, they continue to follow the same simple power laws with Re as the ones for small through flow: When μ is well away from the location μ_2 of the unperturbed pitchfork bifurcation as in Figs. 4(a)–4(c), one has $S=S^{(0)}+S^{(2)}\,\mathrm{Re}^2$, $D=D^{(1)}\,\mathrm{Re}+D^{(3)}\,\mathrm{Re}^3$. On the other hand, at μ_2, as in Figs. 4(d)–4(f) one has $S=S^{(0)}+S^{(2/3)}(\mathrm{Re}^{1/3})^2+S^{(4/3)}(\mathrm{Re}^{1/3})^4$, $D=D^{(1/3)}\,\mathrm{Re}^{1/3}+D^{(1)}\times(\mathrm{Re}^{1/3})^3$. The lines in Fig. 4 show fits of the data from the full numerical simulations (symbols) to these power-law expansions for S and D. Figures 4(c) and 4(f) show plots of the resulting squared moduli $|A|^2=S+D$ and $|B|^2=S-D$.

Note that inversion symmetry $z \leftrightarrow -z$ implies $S(-\mathrm{Re})=S(\mathrm{Re})$ and $D(-\mathrm{Re})=-D(\mathrm{Re})$. For $\mathrm{Re}>0(\mathrm{Re}<0)$ the RIB state is transformed into a L-CR-SPI (R-CR-SPI) with A (B) being the major mode and B (A) the minor one. With increasing through flow the major (minor) mode of the CR-SPI increases (decreases) until the minor mode vanishes in the transition to a pure SPI.

Conclusion. A small applied flow is an inversion-symmetry-breaking perturbation for fluid wave structures that is easy to control. It significantly changes the bifurcation and stability transfer scenario involving symmetry degenerate TWs, mirror symmetric SWs, and mixed wave patterns. Numerical simulations of such waves in the counter-rotating Taylor-Couette system are explained and reproduced quantitatively by amplitude equations containing quintic order coupling and symmetry-breaking perturbation terms. This approach can be applied to a wide range of O(2) symmetric oscillatory instabilities in the presence of inversion-symmetry-breaking perturbations.

This work was supported by the Deutsche Forschungsgemeinschaft.

[1] M. C. Cross and P. C. Hohenberg, Rev. Mod. Phys. **65**, 851 (1993).
[2] R. Tagg, Nonlinear Sci. Today **4**, 1 (1994).
[3] P. Chossat and G. Iooss, *The Couette-Taylor Problem* (Springer, Berlin, 1994).
[4] Ch. Hoffmann, M. Lücke, and A. Pinter, Phys. Rev. E **69**, 056309 (2004).
[5] Y. Demay and G. Iooss, J. Mec. Theor. Appl. 193 (1984), special supplement.
[6] A. Pinter, M. Lücke, and Ch. Hoffmann, Phys. Rev. Lett. **96**, 044506 (2006).
[7] R. Tagg, W. S. Edwards, H. L. Swinney, and P. S. Marcus, Phys. Rev. A **39**, 3734 (1989).
[8] J. Langenberg, G. Pfister, and J. Abshagen, Phys. Rev. E **68**, 056308 (2003).
[9] J. D. Crawford and E. Knobloch, Nonlinearity **1**, 617 (1988).
[10] K. Bühler and N. Polifke, in *Nonlinear Evolution of Spatiotemporal Structures in Dissipative Continuous Systems*, edited by F. Busse and L. Kramer (Plenum Press, New York, 1990), p. 21.
[11] R. Raffaï and P. Laure, Eur. J. Mech. B/Fluids, **12**, n° 3, 277–288 (1993).
[12] M. Avila, A. Meseguer, and F. Marques, Phys. Fluids **18**, 064101 (2006).
[13] $b=-2.45\times10^{-3}$, $c=-1.06\times10^{-2}$, $e=-3.25\times10^{-2}$, $\mu^{(1)}=2.27\times10^{-3}$, $c^{(1)}=2.8\times10^{-2}$.